ISSN 1674-1056
http://cpb.iphy.ac.cn
http://iopscience.iop.org/cpb
中国物理 B
Chinese Physics
中国物理
Chinese Physics B

Coulomb-dominated oscillations in a graphene quantum Hall Fabry-Pérot interferometer

Guan-Qun Zhang(张冠群)[1], Li Lin(林立)[2], Hailin Peng(彭海琳)[2], Zhongfan Liu(刘忠范)[2], Ning Kang(康宁)[1], Hong-Qi Xu(徐洪起)[1,3]

Citation: Chin. Phys. B . 2019, 28(12): 127203 . **doi:** 10.1088/1674-1056/ab55d3
Journal homepage: http://cpb.iphy.ac.cn; http://iopscience.iop.org/cpb

What follows is a list of articles you may be interested in

Magnetotransport properties of graphene layers decorated with colloid quantum dots

Ri-Jia Zhu(朱日佳), Yu-Qing Huang(黄雨青), Jia-Yu Li(李佳玉), Ning Kang(康宁), Hong-Qi Xu(徐洪起)
Chin. Phys. B . 2019, 28(6): 067201 . **doi:** 10.1088/1674-1056/28/6/067201

Valley-polarized pumping current in zigzag graphene nanoribbons with different spatial symmetries

Zhizhou Yu(俞之舟), Fuming Xu(许富明)
Chin. Phys. B . 2018, 27(12): 127203 . **doi:** 10.1088/1674-1056/27/12/127203

The magneto-thermoelectric effect of graphene with intra-valley scattering

Wenye Duan(段文晔), Junfeng Liu(刘军丰), Chao Zhang(张潮), Zhongshui Ma(马中水)
Chin. Phys. B . 2018, 27(9): 097204 . **doi:** 10.1088/1674-1056/27/9/097204

Electro-statically controllable graphene local heater

Hui-Shan Wang(王慧山), Lian-Wen Deng(邓联文), Lei Li(李蕾), Qiu-Juan Sun(孙秋娟), Hong Xie(谢红), Hao-Min Wang(王浩敏)
Chin. Phys. B . 2018, 27(3): 037203 . **doi:** 10.1088/1674-1056/27/3/037203

Transport properties in monolayer-bilayer-monolayer graphene planar junctions

Kai-Long Chu(储开龙), Zi-Bo Wang(王孜博), Jiao-Jiao Zhou(周娇娇), Hua Jiang(江华)
Chin. Phys. B . 2017, 26(6): 067202 . **doi:** 10.1088/1674-1056/26/6/067202

RAPID COMMUNICATION

Coulomb-dominated oscillations in a graphene quantum Hall Fabry–Pérot interferometer*

Guan-Qun Zhang(张冠群)[1], Li Lin(林立)[2], Hailin Peng(彭海琳)[2], Zhongfan Liu(刘忠范)[2], Ning Kang(康宁)[1,†], and Hong-Qi Xu(徐洪起)[1,3,‡]

[1] *Beijing Key Laboratory of Quantum Devices, Key Laboratory for the Physics and Chemistry of Nanodevices and Department of Electronics, Peking University, Beijing* 100871, *China*

[2] *Center for Nanochemistry, Beijing Science and Engineering Center for Nanocarbons, Beijing National Laboratory for Molecular Sciences, College of Chemistry and Molecular Engineering, Peking University, Beijing* 100871, *China*

[3] *Beijing Academy of Quantum Information Sciences, Beijing* 100193, *China*

(Received 23 September 2019; revised manuscript received 30 October 2019; published online 29 November 2019)

The electronic Fabry–Pérot interferometer operating in the quantum Hall regime may be a promising tool for probing edge state interferences and studying the non-Abelian statistics of fractionally charged quasiparticles. Here we report on realizing a quantum Hall Fabry–Pérot interferometer based on monolayer graphene. We observe resistance oscillations as a function of perpendicular magnetic field and gate voltage both on the electron and hole sides. Their Coulomb-dominated origin is revealed by the positive (negative) slope of the constant phase lines in the plane of magnetic field and gate voltage on the electron (hole) side. Our work demonstrates that the graphene interferometer is feasible and paves the way for the studies of edge state interferences since high-Landau-level and even denominator fractional quantum Hall states have been found in graphene.

Keywords: graphene, electronic Fabry–Pérot interferometer, quantum Hall effect, edge state interference

PACS: 72.80.Vp, 73.23.–b, 73.43.–f, 85.35.Ds **DOI:** 10.1088/1674-1056/ab55d3

1. Introduction

An electronic Fabry–Pérot interferometer constructed of two narrow constrictions and a central confined region can be operated in the quantum Hall regime to manipulate the edge states and thus is a good tool to study quantum interference.[1–5] Especially, it is predicted to be able to demonstrate non-Abelian statistics of fractionally charged quasiparticle excitations,[6,7] which may be useful in fault-tolerant topological quantum computation.[8–10]

With a perpendicular magnetic field applied to such an interferometer, edge states will form and travel along the circumference of the device while the quasiparticle states inside the central region are localized owing to the quantum Hall effect. Such edge states are ballistic one-dimensional channels with suppressed backscattering of disorders.[11] The resistance oscillations emerge due to weak tunneling of the edge states at the constrictions and reveal two distinct types of behaviors which have been investigated both experimentally[1,2,4,12–15] and theoretically.[16,17] In large interferometers up to tens μm^2 in size, the constant phase lines in the magnetic field and gate voltage plane have a negative slope which is attributed to the Aharonov–Bohm (AB) effect in the framework of noninteracting electrons.[1,2] Under this circumstance, an edge state which is partially transmitted when penetrating through the constrictions is scattered by the constrictions and changes direction to the opposite edge. The backscattered edge states from the two constrictions interfere. The periodicity of resistance oscillations arises from the phase difference between the two interfering paths which is given by the AB phase, and the magnetic field oscillation period is determined by the flux quantum $\phi_0 = h/e$ and the area of the interference loop A as ϕ_0/A. While in small interferometers up to a few μm^2 in size,[1,4,15,18] the constant phase lines in the two-dimensional plot of magnetic field and gate voltage have a positive slope in contrast. This is because the Coulomb interaction starts to play an important role and thus the interferences display Coulomb-dominated (CD) features of single electron charging.[16,17] Suppressing the Coulomb interaction by inducing effective screening[5,13,14] or making the constriction more open,[3] the AB dominated interferences could also be observed in small interferometers. To our knowledge, previous works on electronic Fabry–Pérot interferometer realized by etching of mesa[4,18] or gating[1,2,14] exclusively focused on the conven-

*Project supported by the National Key Research and Development Program of China (Grant Nos. 2016YFA0300601 and 2017YFA0303304), the National Natural Science Foundation of China (Grant Nos. 11874071, 11774005, and 11974026), and Beijing Academy of Quantum Information Sciences, China (Grant No. Y18G22).

†Corresponding author. E-mail: nkang@pku.edu.cn

‡Corresponding author. E-mail: hqxu@pku.edu.cn

© 2019 Chinese Physical Society and IOP Publishing Ltd

tional two-dimensional electron gas (2DES) systems but few interferometer works based on graphene were reported. It is attractive to study edge state interferences in graphene through such interferometers since high-Laudau-level fractional quantum Hall effect[19–22] and even denominator fractional quantum Hall states have been found in graphene.[23,24]

In this paper, we report on the realization of a quantum Hall Fabry–Pérot interferometer fabricated on a relativistic 2D material — monolayer graphene. The edge state interferences were carefully investigated by the periodic resistance oscillations in the integer quantum Hall regime. We observed CD oscillations near integer quantum Hall plateaus in the graphene interferometer both on the electron side and hole side. Our work takes the first step to study the interference in a graphene quantum Hall interferometer and paves the way to measure the fractionally charged quasiparticle excitations in graphene.

2. Experiments

The device was fabricated from chemical vapor deposition (CVD)-grown high quality monolayer graphene.[25] The starting procedure of fabrication was to transfer CVD-grown graphene onto the heavily doped silicon substrate with a 300 nm silicon oxide coating layer. The interferometer geometry was then defined by electron beam lithography (EBL) and subsequent reactive ion etching (RIE) with oxygen plasma. Finally, Ti/Au bilayer (10 nm/90 nm) contact electrodes were fabricated by an additional EBL procedure and electron beam evaporation (EBE). Figure 1(a) is the atomic force microscope (AFM) image of a device before depositing the electrodes. The bright yellow region is graphene, while the dark region is the silicon oxide substrate where graphene was etched out. The device consists of a interferometer and a standard Hall bar structure. Figure 1(b) is the zoom in of the interferometer in Fig. 1(a). It is constructed with two adjacent narrow constrictions, each of which can scatter the propagating edge state to the opposite edge, and a confined cavity between the constrictions. The interferometer is tuned by the back gate and in-plane side gates L1 and L2. Figure 1(c) is the schematic of edge state paths in the CD regime assuming that the outer edge state (close to the boundary) is fully transmitted at the constriction. The inner edge state is partially transmitted when electrons (holes) enter the central region by weak forward tunneling which is denoted by the horizontal dashed lines.

The measurement of a graphene interferometer with lithographic area of 0.8 μm^2 was conducted in a ^{3}He/^{4}He dilution refrigerator at temperature $T = 60$ mK, with a magnetic field B applied perpendicular to the graphene plane. The diagonal resistance $R_D = V_{47}/I$ of the interferometer and Hall resistance $R_{XY} = V_{59}/I$ of the bulk were measured simultaneously by driving current I from contact 1 to 2 and measuring the voltage drop V_{47} (V_{59}) between contacts 4 and 7 (5 and 9) using a lock-in technique with a current bias $I = 10$–100 nA at 13 Hz.

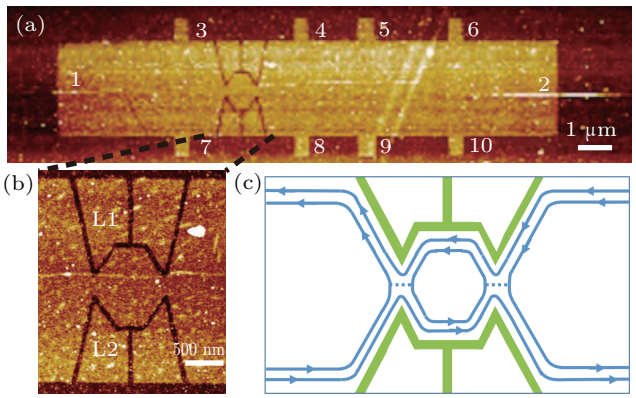


Fig. 1. (a) AFM image of a typical device used in this study. Bright yellow region is graphene and dark region is silicon oxide substrate. It consists of a interferometer and a standard Hall bar structure. Diagonal resistance R_D (between contacts 4 and 7) of the interferometer and Hall resistance R_{XY} (between contacts 5 and 9) of the bulk were measured simultaneously while driving current from 1 to 2. (b) A zoom in of the interferometer in (a). It is constructed with two adjacent narrow constrictions, introducing inter-edge scattering, and a central confined cavity. The designed area of the cavity is about 0.8 μm^2. The side gates labeled by L1 and L2 define the interference path. (c) Schematic of the Coulomb-dominated interference. Propagating edge states are marked by the lines with arrows along the device edge. For the sake of simplicity, this picture (not exact the same in real measurement) shows that only one outer edge (close to the device boundary) is fully transmitted at the constriction. The inner edge state is partially transmitted to the central region by weak forward tunneling which is denoted by the horizontal dashed lines.

3. Results and discussion

Figure 2(a) shows R_D and R_{XY} as a function of back gate voltage V_{BG} with side gates L1 and L2 set to zero and magnetic field $B = 6$ T. R_D and R_{XY} display quantized integer Hall plateaus at filling factor $\nu = \pm 4(n + 1/2)$, $n = 0$, 1, 2, where $\pm$ represents electrons and holes, respectively, which is typical for monolayer graphene in the quantum Hall regime. R_D exhibits obvious resistance oscillations in contrast to R_{XY} which shows no such oscillatory feature. Figure 2(b) is a zoom in of the typical resistance oscillations near $\nu = -6$ in Fig. 2(a). ΔR_D is the measured R_D with the smooth background subtracted. The inset of Fig. 2(b) displays the result of fast Fourier transform (FFT) performed on the oscillatory ΔR_D. The spectrum of FFT shows a sharp peak at a single frequency, demonstrating that the oscillations are periodic in back gate voltage. ΔR_D is then measured as a function of the magnetic field, with $V_{BG} = -12.5$ V (near $\nu = -10$) and side gates L1 and L2 set to zero. The results are shown in Fig. 2(c). Again, the FFT of the oscillations in the inset shows a single sharp peak, which indicates the good periodicity in magnetic field. The origin of these oscillations is investigated below.

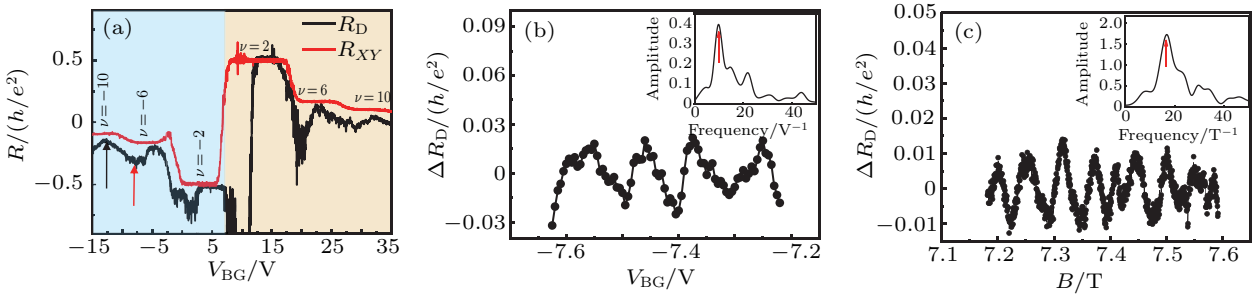


Fig. 2. (a) Diagonal resistance R_D (black curve) and Hall resistance R_{XY} (red curve) as a function of back gate voltage under perpendicular magnetic field $B = 6$ T with side gates L1 and L2 set to zero. Numbered horizontal lines indicate well developed quantum Hall plateaus. Orange (blue) shaded area corresponds to electron (hole) carriers. (b) Zoom in of the resistance oscillations in (a) (highlighted by the red arrow). ΔR_D is the measured R_D with the gross background subtracted, showing oscillations at near filling factor $\nu = -6$. Inset: the FFT of the ΔR_D data which shows a sharp peak at a single frequency, demonstrating the oscillations are periodic in back gate voltage. (c) ΔR_D as a function of perpendicular magnetic field B around $\nu = -10$ at $V_{BG} = -12.5$ V (denoted by the black arrow in (a)) with side gates L1 and L2 set to zero. Inset: the FFT results of the oscillations which shows a sharp peak at a single frequency, indicating the good periodicity in magnetic field.

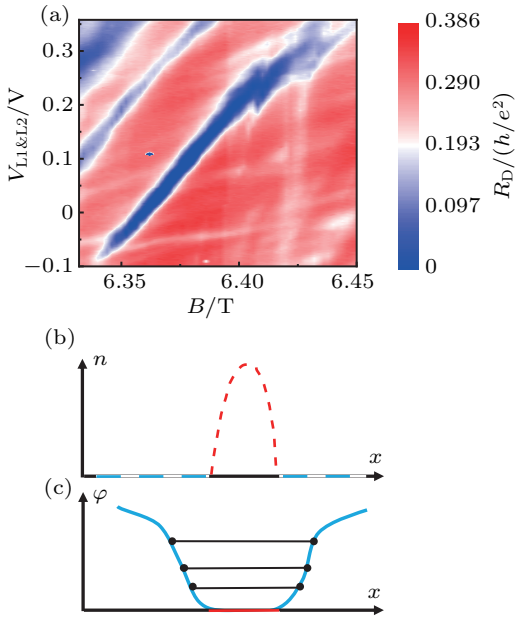


Fig. 3. R_D as a function of B and $V_{L1\&L2}$ with back gate voltage $V_{BG} = 17.4$ V near $\nu = 2$. $V_{L1\&L2}$ is the gate voltage applied on side gates L1 and L2 which are jointed together. Note that here the carrier type is electron. The positive slope of the constant phase lines indicates that the interference is Coulomb-dominated. Magnetic period $\Delta B \approx 45$ mT corresponds to an area $A \approx 0.046$ μm^2. It gives a mean interfering area with radius ~ 120 nm, which is smaller than the lithographic geometry. (b) Schematic profile of spatial carrier density distribution when starting to fill an empty Landau level. Red dashed lines represent carrier density in compressible region while blue dashed lines represent incompressible region. (c) The corresponding screened disorder potential of (b). Red solid line denotes the compressible region where the disorder potential is screened while blue solid lines denote incompressible region where the potential is unscreened. Thus, the compressible region acts as a Coulomb island, the size and position of which are determined by the details of the disorder potential. For clarity, only one non-degenerate Landau level is considered.

Resistance oscillations in the quantum Hall interferometer observed in previous experimental works focusing on conventional 2DES are either interpreted to base on the CD charing effect[1,4,15,18] or attributed to the AB interference.[1–3,5,13,14] One of the distinct features to distinguish these two regimes is that the constant phase lines in the magnetic field and gate voltage plane have a positive (negative) slope for the CD (AB) oscillations. Thus, in Fig. 3(a), we show R_D as a function of magnetic field B and side gate voltage $V_{L1\&L2}$ at $V_{BG} = 17.4$ V near $\nu = 2$, $V_{L1\&L2}$ is the gate voltage applied on side gates L1 and L2 which are jointed together. The reason we choose filling factor $\nu = 2$ is that at higher filling factor, larger numbers of edge states with finite width[26] result in counter-propagating edge states in close proximity inside the narrow constrictions[27] which causes the edge states to be mixed by tunneling through the localized states arising from disorders and thus decreases the visibility of the interference. Note that here the type of carrier is electron. The constant phase lines exhibit a positive slope which is consistent with the small sized interferometers being in CD regime, indicating their CD interference origin.

Having identified the CD regime, we introduce a qualitative description of this regime in the next to analyze the data. Assume both bulk and central confined region of the interferometer include an incompressible region with f_0 fully occupied Landau levels. Inside the central region, filling factor higher than f_0 with partially occupied Landau level will form a compressible region which is surrounded by the incompressible region. Electrons residing in the compressible region behave as a quasi-isolated Coulomb island and vary discretely.

The magnetic field varies the flux of the central region in the form $\delta\phi = A\delta B + B\delta A'$, where A is the area of the interference loop, and $\delta A'$ is the interaction induced area response caused by the coupling between the Coulomb island and edge states. When a whole flux quantum ϕ_0 is added to the central region, the occupation of electrons within Landau levels will redistribute by adding one electron into every fully filled Landau level and thus totally f_0 electrons into all fully occupied Landau levels. At the meantime, f_0 electrons must be moved out from the compressible region due to the Coulomb interaction. Thus, increasing magnetic field plays an role like applying more negative voltage of a gate which electrostatically couples to the Coulomb island. The magnetic field also has impact on the interference area in an observable way. In

the process that the magnetic field increases, the area of interference loop A first shrinks by $\delta A'$ to keep constant flux and abruptly recovers to the original area A with $\delta A' = 0$ when $\delta\phi$ reaches ϕ_0.[14]

For an ideal back gate, it influences the resistance oscillations through its effect on the carrier density. For example, the oscillation period in back gate voltage in Fig. 2(b) corresponds to a single electron added to the Coulomb island through capacitive coupling. For an ideal side gate, it varies the enclosed flux by slowly affecting the interference area A. Therefore, considering all the contributions above to the Coulomb blockade effect, the charging energy of the Coulomb island is determined by

$$E_c = \frac{1}{2C}(ef_0 \cdot \delta BA/\phi_0 + eN - C_g V_g)^2, \tag{1}$$

where C is the total capacitance of the Coulomb island, N is the integer number of electrons hopping into or out the Coulomb island, V_g is the gate voltage, and C_g which is the capacitance between the gate and the Coulomb island. The magnetic field oscillation period $\Delta B \approx 45$ mT in Fig. 3(a) corresponds to an area of the interference loop $A \approx 0.046$ μm^2 according to $\Delta B = \phi_0/(f_0 A)$ deduced from Eq. (1).[16] The mean radius of the Coulomb island should be ~ 120 nm, which is smaller than the lithographic radius of the interferometer. To explain this inconsistence, we refer to the localization of 2DES in a disorder potential within the quantum Hall regime. It is worth ignoring Coulomb interaction and screening effect at first, that is, in the single-particle[28] picture of localization under quantum Hall conditions, each localized state consists of a constant energy orbit of the disorder potential and contains integer number of flux quantum. When increasing the magnetic field, the constant energy orbit will shrink to keep the constant flux. In view of that the degeneracy of the Landau level $n_{\max} = B/\phi_0$ is also increased, the number of localized states is increased accordingly. While taking the Coulomb interaction and screening effect into consideration in the quantum Hall regime, localization is no longer dominated by single-particle physics and the number of localized states stays unchanged both in conventional 2DES[29] and graphene.[30,31]

In detail, carrier density n does not uniformly distribute in space but fluctuates in an inhomogeneous profile to screen the bare disorder potential. Figures 3(b) and 3(c) illustrate this scenario schematically. The dashed line in Fig. 3(b) indicates the profile of the carrier density. Assuming electrons start to fill an empty Landau level in Fig. 3(b), near the bottoms of the profile of carrier density n, the Landau level is completely empty ($n = 0$) and forms local incompressible regions (blue dashed line) within which no electron can be used to redistribute to screen the bare disorder potential. Where $n > 0$, the Landau level is partially filled and there are available states for electrons to rearrange to screen the disorder potential where a compressible region forms (red dashed line). Accordingly, in Fig. 3(c), the bare disorder potential is screened in the compressible region (red solid line), while in the incompressible region (blue solid line) the potential sticks out and forms a potential valley. When the compressible region is surrounded by an incompressible region, it acts as a localized Coulomb island and electron transport is dominated by Coulomb blockade physics. Therefore, the reason that the area of Coulomb island in Fig. 3(a) is smaller than the designed area may be attributed to the formation of the localized compressible region which is determined by the details of the disorder potential. This interpretation is further corroborated by the experiment of a quantum Hall interferometer studied by scanning gate microscopy (SGM)[32] which demonstrates that the Coulomb island could exist anywhere inside the central region and an experiment in graphene nanoribbons in the quantum Hall regime which verifies that the single quantum dot forms.[31]

Up to now, we have discussed the CD oscillations on the electron side. Next, oscillations for holes are investigated. Figure 4 shows the plots of resistance oscillations in the B–$V_{L1\&L2}$ plane, with back gate voltage $V_{BG} = -1$ V on the hole side near $\nu = -2$. To clarify, we point out here that the effect of gating for holes is contrary to that for electrons. Hence, the constant phase lines which have a negative slope in Fig. 4 are consistent with the CD mechanism rather than the AB mechanism. The oscillation period in magnetic field $\Delta B \approx 7.5$ mT and the corresponding area of the Coulomb island is about 0.267 μm^2, which gives a mean radius $R \approx 300$ nm. Again, it is smaller compared to the lithographic area of the interferometer which can be explained in the same framework discussed above. But it is worth noting that the area of the Coulomb island here is different from the area of electron carrier. The inherent electron–hole asymmetry in graphene[33–38] may be possibly responsible for this scenario. To verify this, we compare the width of $\nu = 2$ plateau and that of $\nu = -2$ plateau in Fig. 2(a), deducing that the dominated disorder potential is negatively charged because repulsive Coulomb potential leads to smaller scattering rate for the Dirac fermions in graphene[33,36–38] which corresponds to the lager width of plateau for electrons. For a negative disorder potential, the localized density of states below (above) the Dirac point is enhanced (reduced).[34,35] Accordingly, the screening effect of the disorder potential in the process of localization under quantum Hall conditions will be much stronger on the hole side than that on the electron side. Thus, the Coulomb island seen by holes will be larger than that by electrons.

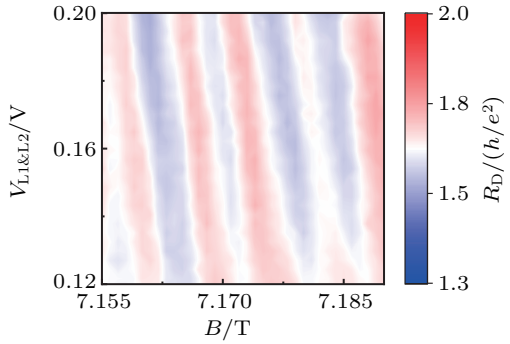


Fig. 4. Plots of R_D in the B–$V_{L1\&L2}$ plane, with back gate voltage $V_{BG} = -1$ V near $\nu = -2$. Note here the carrier type is hole. The negative slope of the constant phase lines indicates the device being in the CD regime (for electron carriers, negative slope represents Aharonov–Bohm interference). The magnetic field oscillation period $\Delta B \approx 7.5$ mT corresponds to an interference loop with area $A \approx 0.276$ μm^2 which has a mean radius of ~ 300 nm.

4. Conclusion

Our work takes the first step to study the edge state interferences in the graphene quantum Hall interferometer. The principle finding of this work is that the resistance oscillations on both the electron and hole sides are in the CD regime. We propose that the next-step experiment could encapsulate graphene in hexagonal boron nitride together with a graphite back gate to reduce the influence of external disorder potential.[39,40] Since high-Laudau-level[19–22] and even denominator[23,24] fractional quantum Hall effect have been found in graphene, we expect that the graphene interferometer will offer an intriguing platform for future studies of non-Abelian statistics.

References

[1] Zhang Y, McClure D T, Levenson-Falk E M, Marcus C M, Pfeiffer L N and West K W 2009 *Phys. Rev. B* **79** 241304
[2] McClure D T, Zhang Y, Rosenow B, Levenson-Falk E M, Marcus C M, Pfeiffer L and West K W 2009 *Phys. Rev. Lett.* **103** 206806
[3] Willett R L, Pfeiffer L N and West K 2010 *Phys. Rev. B* **82** 205301
[4] McClure D, Chang W, Marcus C M, Pfeiffer L and West K 2012 *Phys. Rev. Lett.* **108** 256804
[5] Nakamura J, Fallahi S, Sahasrabudhe H, Rahman R, Liang S, Gardner G C and Manfra M J 2019 *Nat. Phys.* **15** 563
[6] Bonderson P, Kitaev A and Shtengel K 2006 *Phy. Rev. Lett.* **96** 016803
[7] Ilan R, Grosfeld E and Stern A 2008 *Phys. Rev. Lett.* **100** 086803
[8] Kitaev A Y 2003 *Annals of Physics* **303** 2
[9] Nayak C, Simon S H, Stern A, Freedman M and Sarma S D 2008 *Rev. Mod. Phys.* **80** 1083
[10] Willett R 2013 *Rep. Prog. Phys.* **76** 076501
[11] Datta S 1997 *Electronic transport in mesoscopic systems* (Cambridge: Cambridge University Press)
[12] Ofek N, Bid A, Heiblum M, Stern A, Umansky V and Mahalu D 2010 *Proc. Natl. Acad. Sci. USA* **107** 5276
[13] Choi H K, Sivan1 I, Rosenblatt1 A, Heiblum M, Umanskyl V and Mahalu1 D 2015 *Nat. Commun.* **6** 7435
[14] Sivan I, Choi1 H K, Park1 J, Rosenblattl A, Gefen1 Y, Mahalul D and Umansky V 2016 *Nat. Commun.* **7** 12184
[15] Zhu Y Y, Bai M M, Zheng S Y, Fan J, Jing X N, Ji Z Q, Yang C L, Liu G T and Lu L 2017 *Chin. Phys. Lett.* **34** 067301
[16] Rosenow B and Halperin B 2007 *Phys. Rev. Lett.* **98** 106801
[17] Halperin B I, Stern A, Neder I and Rosenow B 2011 *Phys. Rev. B* **83** 155440
[18] Camino F, Zhou W and Goldman V 2007 *Phys. Rev. B* **76** 155305
[19] Du X, Skachko I, Duerr F, Luican A and Andrei E Y 2009 *Nature* **462** 192
[20] Dean C R, Young A F, Cadden-Zimansky P, Wang L, Ren H, Watanabe K, Taniguchi T, Kim P, Hone J and Shepard K 2011 *Nat. Phys.* **7** 693
[21] Lin X, Du R and Xie X 2014 *Natl. Sci. Rev.* **1** 564
[22] Amet F, Bestwick A, Williams J, Balicas L, Watanabe K, Taniguchi T and Goldhaber-Gordon D 2015 *Nat. Commun.* **6** 5838
[23] Zibrov A, Spanton E, Zhou H, Kometter C, Taniguchi T, Watanabe K and Young A 2018 *Nat. Phys.* **14** 930
[24] Kim Y, Balram A C, Taniguchi T, Watanabe K, Jain J K and Smet J H 2019 *Nat. Phys.* **15** 154
[25] Lin L, Li J, Ren H, Koh A L, Kang N, Peng H, Xu H Q and Liu Z 2016 *ACS Nano* **10** 2922
[26] Chklovskii D, Shklovskii B I and Glazman L 1992 *Phys. Rev. B* **46** 4026
[27] Aoki N, Da Cunha C, Akis R, Ferry D and Ochiai Y 2005 *Phys. Rev. B* **72** 155327
[28] Huckestein B 1995 *Rev. Mod. Phys.* **67** 357
[29] Ilani S, Martin J, Teitelbaum E, Smet J, Mahalu D, Umansky V and Yacoby A 2004 *Nature* **427** 328
[30] Martin J, Akerman N, Ulbricht G, Lohmann T, Von Klitzing K, Smet J and Yacoby A 2009 *Nat. Phys.* **5** 669
[31] Tóvári E, Makk P, Rickhaus P, Schönenberger C and Csonka S 2016 *Nanoscale* **8** 11480
[32] Hackens B, Martins F, Faniel S, Dutu C A, Sellier H, Huant S, Pala M, Desplanque L, Wallart X and Bayot V 2010 *Nat. Commun.* **1** 39
[33] Novikov D 2007 *Appl. Phys. Lett.* **91** 102102
[34] Wang Y, Brar V W, Shytov A V, Wu Q, Regan W, Tsai H Z, Zettl A, Levitov L S and Crommie M F 2012 *Nat. Phys.* **8** 653
[35] Wang Y, Wong D, Shytov A V, Brar V W, Choi S, Wu Q, Tsai H Z, Regan W, Zettl A, Kawakami R K, *et al.* 2013 *Science* **340** 734
[36] Bai K K, Wei Y C, Qiao J B, Li S Y, Yin L J, Yan W, Nie J C and He L 2015 *Phys. Rev. B* **92** 121405
[37] Srivastava P K, Arya S, Kumar S and Ghosh S 2017 *Phys. Rev. B* **96** 241407
[38] Li J, Lin L, Rui D, Li Q, Zhang J, Kang N, Zhang Y, Peng H, Liu Z and Xu H 2017 *ACS Nano* **11** 4641
[39] Overweg H, Eggimann H, Chen X, Slizovskiy S, Eich M, Pisoni R, Lee Y, Rickhaus P, Watanabe K, Taniguchi T, *et al.* 2017 *Nano Lett.* **18** 553
[40] Banszerus L, Frohn B, Epping A, Neumaier D, Watanabe K, Taniguchi T and Stampfer C 2018 *Nano Lett.* **18** 4785